Biology of Reproduction, 2019, 101(4), 782–790
doi:10.1093/biolre/ioz126
Research Article
Advance Access Publication Date: 18 July 2019

OXFORD

Research Article

Association of luteal cell degeneration and progesterone deficiency with lysosomal storage disorder mucolipidosis type IV in *Mcoln1*$^{-/-}$ mouse model†

Zidao Wang[1,2,‡], Ahmed E. El Zowalaty[1,2,‡], Yuehuan Li[1], Christian L. Andersen[1,2] and Xiaoqin Ye[1,2,*]

[1]Department of Physiology and Pharmacology, College of Veterinary Medicine, University of Georgia, Athens, Georgia, USA; and [2]Interdisciplinary Toxicology Program, University of Georgia, Athens, Georgia, USA.

***Correspondence**: Department of Physiology and Pharmacology, College of Veterinary Medicine; Interdisciplinary Toxicology Program, University of Georgia, 501 DW Brooks Dr., Athens, Georgia 30602, USA. Tel: 1-706-542-6745; E-mail: ye@uga.edu

† **Grant Support**: NIH R01HD065939 and R03HD097384 (XY).

‡These authors contributed equally to the work.

Received 21 December 2018; Revised 13 April 2019; Accepted 11 July 2019

Abstract

Transient receptor potential cation channel, mucolipin subfamily, member 1 (TRPML1) (*MCOLN1*/*Mcoln1*) is a lysosomal counter ion channel. Mutations in *MCOLN1* cause mucolipidosis type IV (MLIV), a progressive and severe lysosomal storage disorder with a slow onset. *Mcoln1*$^{-/-}$ mice recapitulate typical MLIV phenotypes but roles of TRPML1 in female reproduction are unknown. Despite normal mating activities, *Mcoln1*$^{-/-}$ female mice had reduced fertility at 2 months old and quickly became infertile at 5 months old. Progesterone deficiency was detected on 4.5 days post coitum/gestation day 4.5 (D4.5). Immunohistochemistry revealed TRPML1 expression in luteal cells of wild type corpus luteum (CL). Corpus luteum formation was not impaired in 5–6 months old *Mcoln1*$^{-/-}$ females indicated by comparable CL numbers in control and *Mcoln1*$^{-/-}$ ovaries on both D1.5 and D4.5. In the 5–6 months old *Mcoln1*$^{-/-}$ ovaries, histology revealed less defined corpus luteal cord formation, extensive luteal cell vacuolization and degeneration; immunofluorescence revealed disorganized staining of collagen IV, a basal lamina marker for endothelial cells; Nile Red staining detected lipid droplet accumulation, a typical phenotype of MLIV; immunofluorescence of heat shock protein 60 (HSP60, a mitochondrial marker) and *in situ* hybridization of steroidogenic acute regulatory protein (StAR, for the rate-limiting step of steroidogenesis) showed reduced expression of HSP60 and StAR, indicating impaired mitochondrial functions. Luteal cell degeneration and impaired mitochondrial functions can both contribute to progesterone deficiency in the *Mcoln1*$^{-/-}$ mice. This study demonstrates a novel function of TRPML1 in maintaining CL luteal cell integrity and function.

Summary Sentence

Our finding that *Mcoln1*$^{-/-}$ female mice have luteal cell degeneration and progesterone deficiency reveals a novel role of TRPML1 in luteal cell survival and function.

Key words: TRPML1/*Mcoln1*, corpus luteum, progesterone, lipid accumulation, heat shock protein 60, StAR

Introduction

Transient receptor potential cation channel, mucolipin subfamily, member 1 (TRPML1) belongs to the superfamily of transient receptor potential (TRP) channels, which includes ~30 members. The mucolipin subfamily of TRP channels has three members, TRPML1-3, which are tetrameric six-transmembrane channels. TRPML1 is encoded by mucolipin 1 (*MCOLN1*, *Mcoln1*). It is localized in the membrane of late endosomes and lysosomes to regulate lumen acidity [1]. Lysosomal acidity is critical for the activities of lysosomal enzymes and it is mainly maintained by vacuolar-type H^+-ATPase (V-ATPase), which pumps H^+ into lysosomal lumen, and counter ion channels, which dissipate the transmembrane voltage built up by V-ATPase [1–3]. TRPML1 exerts its function as a counter ion channel by mediating the release of Ca^{2+}, Na^+, Fe^{2+}, and potentially other cations from the lysosomal lumen to cytosol [1, 4, 5]. In addition to maintaining an acidic lysosomal lumen, TRPML1 is critical for vesicular trafficking, lipid homeostasis, autophagy, plasma membrane repair, signaling in cellular adaptation to nutrient availability, etc. [4, 5]. TRPML1 deficiency has been associated with mucolipidosis type IV (MLIV) in both humans and mice [1, 6–9]. Mucolipidosis type IV is a type of lysosomal storage disorders, which are inherited metabolic disorders resulting from mutations in lysosomal genes [1, 4, 5]. *Mcoln1*$^{-/-}$ mice recapitulate phenotypes associated with MLIV, such as neurodegeneration, ophthalmologic abnormalities, and muscular dystrophy [7, 9].

Lysosomes have been implicated in multiple events in the ovary, such as follicular atresia, ovulation, steroidogenesis, and luteal regression. Follicular atresia, which starts with the death of granulosa cells and ends with the degeneration of oocytes [10], is an important process to ensure the success of finite ovulation of a few follicles. The lysosome has been implicated in both granulosa cell atresia [11–16], such as lysosomal rupture-induced necrosis [14], and oocyte atresia [17, 18], such as autophagy [17]. Ovulation involves follicle rupture, which is correlated with increased concentration of lysosomal enzymes in the ovarian bursa fluid [19] and increased release of lysosomal enzymes from the epithelium covering the Graafian follicles into the extracellular space [20]. The ovarian hormones (estrogen and progesterone) are produced via steroidogenesis in the follicle (mainly for estrogen synthesis) and corpus luteum (mainly for progesterone synthesis). A major role of lysosomes in steroidogenesis is to release cholesterol, the precursor for steroid hormone synthesis [21], from the cholesterol-lipoprotein complex by lysosomal enzymes [22]. The lysosomes may also regulate steroidogenesis in cultured bovine granulosa cells via controlling the expression of steroidogenic acute regulatory protein (StAR), which carries out the rate-limiting step of steroidogenesis [23]. The corpus luteum (CL) is a temporary endocrine structure developing from granulosa cells and theca cells in the ovulated follicles. It is the main site of progesterone production to support early pregnancy, such as embryo implantation. If pregnancy does not occur or progesterone production in CL is no longer needed during pregnancy, the CL will undergo luteal regression/luteolysis. The success of luteolysis is required to initiate the next estrous cycle in the ovary. Changes in lysosomes (e.g., increased number and size of lysosomes, increased lysosomal enzyme activity) have been implicated in CL regression [24, 25].

Despite the importance of lysosomes in ovary and the critical roles of lysosomal counter ion channels in maintaining lysosomal acidity and functions, the functions of lysosomal counter ion channels in the ovary are unknown. Our group had novel findings that embryo implantation initiation was associated with increased expression of Atpase, H^+ transporting, lysosomal V0 subunit D2 (*Atp6v0d2*, encoding the V0D2 subunit of V-ATPase, which is the proton pump and key regulator of the pH in the lysosomal lumen) [26], and increased lysosomal acidity in the uterine epithelium [27], as well as that uterine receptivity was impaired upon treatment with a V-ATPase inhibitor [27], suggesting the involvement of lysosomes in embryo implantation initiation. Since counter ion channels are important for regulating lysosomal acidity and *Mcoln1* has the highest mRNA expression level in the peri-implantation uterine luminal epithelium among the counter ion channels (GEO number: GSE44451) [26], we hypothesized that TRPML1 was important for embryo implantation, despite an earlier report indicating that *Mcoln1*$^{-/-}$ female mice were fertile [9]. Similar to our previous study on *RhoA*$^{d/d}$ (*RhoA*$^{f/f}$-*Pgr-Cre*$^{+/-}$) mice [28], our systematic study on fertility in the *Mcoln1*$^{-/-}$ female mice led us to the finding that TRPML1 had an important role in the CL for progesterone synthesis, which is essential for embryo implantation.

Materials and methods

Animals and genotyping

Mcoln1 $^{+/-}$ mice were purchased from The Jackson Laboratory (B6.Cg-*Mcoln1*$^{tm1Sasl/J}$ Stock No: 027110 [9]) to generate *Mcoln1*$^{-/-}$ mice and control mice (*Mcoln1*$^{+/+}$ and *Mcoln1*$^{+/-}$). PCR was used for genotyping. Primers P1 (5′-GGGAGTTAAAACAGTG-AAGAAGG-3′) and P3 (5′-CAGTGTGAGGTTCTTGTAACTGG-3′) were used to amplify the wild type allele (195 bp). Primers P2 (5′-CAGCTGGGGCTCGACTAGA-3′) and P3 (5′-CAGTGTGAGGTT-CTTGTAACTGG-3′) were used to amplify the mutant allele (117 bp). All mice were maintained on PicoLab mouse diet 20 and were housed in polypropylene cages with free access to food and water on a 12 h light/dark cycle (0600–1800) at 23 ± 1°C with 30–50% relative humidity. All methods used in this study were approved by the University of Georgia Institutional Animal Care and Use Committee (IACUC) and conform to Guide for the Care and Use of Laboratory Animals.

Mating and fertility tests

Mcoln1 $^{-/-}$ female mice and control mice at 2 months (N = 30/group) and 4 months (N = 10/group) old were mated with wild type stud males. Each stud male was housed with both *Mcoln1*$^{-/-}$ and control females in the same cage. Each female was checked for the presence of a copulation plug every morning to determine mating activity during the previous night. The day of vaginal plug detection was designated as 0.5 days post coitum or gestation day 0.5 (D0.5, mating night as D0). The mated females were separated from the mating males when they showed steady gain of body weight as a positive sign of pregnancy. Some females were plugged multiple times before a term pregnancy was achieved. Plugging latency was defined as the duration from cohabitation to detection of the first copulation plug. Plugging rate was the percentage of mice in each group with the presence of a vaginal plug. Term pregnancy rate was the percentage of mated mice that delivered pups.

Embryo implantation

Five months old *Mcoln1*$^{-/-}$ female mice (N = 7) and control mice (N = 8) were mated with wild type stud males following the same

setting as for the fertility test above. Plugging latency and plugging rate were determined. Embryo implantation was detected on D4.5 (implantation initiation occurs ~D4.0 in mice) between 11:00 and 12:00 h using Evan blue dye injection [27, 29, 30]. Implantation rate was determined as the percentage of plugged mice with implantation sites in each group. Blood was collected via orbital sinus. One ovary was fixed in 10% formalin solution and the other frozen.

Serum P4 and E2 measurement

Serum was collected from the blood samples above (D4.5, 5 months old, N = 7–8) after clotting at room temperature for 45 min and stored at −80°C. Serum progesterone (P4) and 17β-estradiol (E2) were measured in the Ligand Assay and Analysis Core of the Center for Research in Reproduction at the University of Virginia (Charlottesville, Virginia).

Ovary histology

Mcoln1 $^{-/-}$ and control female mice (5–6 months old) were mated with wild type stud males and dissected on D1.5 (N = 4/group). One ovary was fixed in 10% Formalin solution and the other frozen. D4.5 ovaries were from embryo implantation study above. The fixed ovaries were kept in the fixative for 24 h and then transferred to 70% ethanol. They were processed for paraffin embedding as previously described [28, 31, 32]. Paraffin sections (4 μm) through the widest middle portion of the ovaries were collected, processed, and stained with hematoxylin and eosin.

Number of corpora lutea (CLs)

The sections (including those for histology, immunofluorescence, and Nile Red staining) from 5 to 6 months old D1.5 ovaries (N = 4) and D4.5 ovaries (N = 10–20) were independently examined by two individuals for the number of CLs on each section. For the sections with inconsistent counting of CLs (often off by 1), they were reevaluated by the two individuals together to agree on a final number of CLs on each section. The number of CLs from one middle section per ovary per mouse was used for statistical analysis.

Immunohistochemistry and immunofluorescence

Immunohistochemistry was employed to detect TRPML1 in D3.5 wild type ovary using a monoclonal anti-TRPML1 antibody, which was kindly provided by Dr. Abigail A Soyombo [7]. Negative control was processed together except without the primary antibody. The sections were counterstained with hematoxylin. Immunofluorescence was used to detect collagen IV (Col IV) and heat shock protein 60 (HSP60) in the control and *Mcoln1*$^{-/-}$ fixed ovarian sections (4 μm) as previously described [28]. Briefly, paraffin sections were processed and subjected to antigen retrieval in 0.01 M sodium citrate (pH 6.0) at 95°C for 20 min. Sections were washed with 1×PBS followed by membrane permeabilization with 0.15% Triton X-100. The slides were then washed and blocked with 10% goat serum for 1 h at room temperature and incubated with anti-collagen IV (1:200, Abcam, ab19808) or anti-HSP60 (1:400, Cell Signaling Technology, mAb #12165) for overnight at 4°C. The following day, the sections were washed in 1×PBS and incubated with secondary Alexa Fluor 488-conjugated goat anti-rabbit IgG antibody (1:200, Molecular Probes) for 1 h. The sections were counterstained and mounted in DAPI (4′,6′-diamino-2-phenylindole)-containing Vectashield (Vector Laboratories, Burlingame, CA, USA). The immunofluorescence intensities in the CLs and interstitial compartment were quantified using ImageJ (Version 1.51j8) [28]. The relative immunofluorescence intensity in the CLs in each section was calculated as the ratio of the average intensity in all CLs over the intensity in the interstitial compartment on the same section.

In situ hybridization

In situ hybridization of StAR, the rate limiting enzyme in steroidogenesis, in the CLs was performed as we did previously [28].

Lipid droplet staining

Frozen ovarian sections (10 μm) were fixed in 4% paraformaldehyde at room temperature for 20 min, washed twice in 1× PBS, then covered with 1.6 μg/ml Nile red (N3013, Sigma-Aldrich) in 1× PBS at room temperature for 15 min. Sections were then washed in 1× PBS and counterstained with DAPI. The numbers and sizes of lipid droplets were quantified using ImageJ [28]. Briefly, the original images were converted to 8-bit images by using Split Channels. The background subtraction and threshold adjustment with Yen were performed by two individuals, and the averages of the two individual were used for the quantification of lipid droplet numbers and sizes using Analyze Particles in ImageJ.

Statistical analysis

Data are presented as mean ± SD where applicable. Wilcoxon Rank Sum test was used for plugging latency. For parameters with percentage, two-tailed Fisher exact test was used. Two-tailed unequal variance student t-test was used for the other quantitative data. Significance level was set at $P < 0.05$.

Results

Normal mating activity but reduced fertility in *Mcoln1*$^{-/-}$ females

To start the female fertility study, *Mcoln1*$^{-/-}$ female mice and control (*Mcoln1*$^{+/-}$ and *Mcoln1*$^{+/+}$) female mice were mated with the same wild type (WT) stud males. The *Mcoln1*$^{-/-}$ female mice had comparable plugging rate (the percentage of mice in the group with the presence of a vaginal plug) (Figure 1A) and first mating latency (the duration from cohabitation to first mating, indicated by the presence of a vaginal plug) (Figure 1B) as the control females from 2 to 5 months old, indicating normal neuroendocrine function in regulating mating activity in the *Mcoln1*$^{-/-}$ female mice. However, the *Mcoln1*$^{-/-}$ female mice had decreased term pregnancy rate (the percentage of mated females that delivered pups) at both 2 and 4 months old (Figure 1C). The litter sizes from the fertile 2 and 4 months old *Mcoln1*$^{-/-}$ dams were comparable to those from the age-matched control dams (Figure 1D). Because the *Mcoln1*$^{-/-}$ females at >5 months old could be plugged (mated) multiple times but failed to show pregnancy based on post coitum body weight curve, embryo implantation detected on 4.5 days post coitum (D4.5, implantation initiation occurs ~D4.0 in mice) was used as an end point to indicate fertility in >5 months old mice. The implantation rate was 87.5% (7/8) in the control females but 0% (0/7) in the *Mcoln1*$^{-/-}$ females at 5 months old (Figure 1C and D). In addition, six out of these seven *Mcoln1*$^{-/-}$ females had uterine distention (data not shown). The average age at dissection on D4.5 was 22.7 ± 1.5 weeks old (5.3 months old) in control and 22.4 ± 2.0 weeks old (5.2 months old) in *Mcoln1*$^{-/-}$ female mice. These data indicate that although there was a reduced term pregnancy rate, the majority

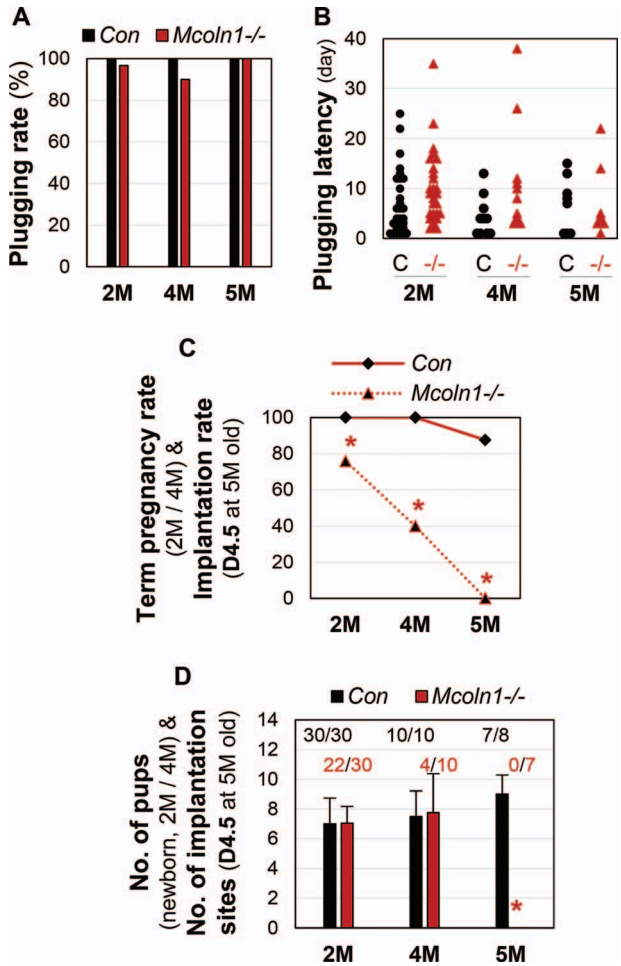

Figure 1. Normal mating activity but impaired fertility in *Mcoln1*$^{-/-}$ female mice. (A) Plugging rate. N = 30 (2M), 10 (4M), or 7–8 (5M). (B) Plugging latency from cohabitation to detection of a vaginal plug. Each black dot (C, control, *Mcoln1*$^{+/+}$ and *Mcoln1*$^{+/-}$) or red triangle (−/−, *Mcoln1*$^{-/-}$): an individual mouse; 2M, 4M, 5M: 2, 4, and 5 months old. (C) Term pregnancy rate (2M, 4M) or implantation rate on gestation day 4.5 (D4.5) (5M) in the mated mice. * $P < 0.05$. (B and C) N = 28–30 (2M), 9–10 (4M), or 7–8 (5M). (D) Number of pups at birth (2M, 4M) or number of implantation sites on 4.5 days post coitum/gestation day 4.5 (D4.5, 5M) in the mated mice. The number on top of each bar: the number of mice delivered pups (2M and 4M) or with implantation sites (5M)/the total number of mated mice in each group; black for control and red for *Mcoln1*$^{-/-}$; * $P < 0.05$; error bar, standard deviation.

(>2/3) of young adult *Mcoln1*$^{-/-}$ female mice were fertile at 2 months old but they quickly became infertile at 5 months old, when the majority of the control females were still fertile.

P4 deficiency in *Mcoln1*$^{-/-}$ females

Since ovarian hormones are critical for embryo implantation, we examined the ovarian hormone levels on these D4.5 mice at 5 months old. The serum progesterone (P4) level in these *Mcoln1*$^{-/-}$ females was significantly reduced, at a level <16% of the control, while there was no significant difference in the serum estrogen (E2) level between these *Mcoln1*$^{-/-}$ females and the control females (Figure 2). These data indicate P4 deficiency in the 5 months old D4.5 *Mcoln1*$^{-/-}$ females.

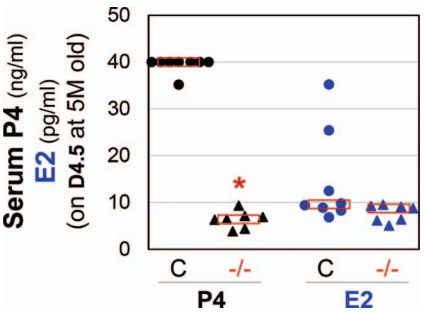

Figure 2. Serum progesterone (P4) and estrogen (E2) levels in D4.5 control and *Mcoln1*$^{-/-}$ female mice at 5 months (5M) old. Each dot or triangle: an individual mouse from fertility test at 5 months old in Figure 1C; black dot or triangle for P4 levels and blue dot or triangle for E2 levels; red rectangle: median for each group; C: control, *Mcoln1*$^{+/+}$ and *Mcoln1*$^{+/-}$, N = 8; −/−: *Mcoln1*$^{-/-}$, N = 7; * $P < 0.05$. Note: seven out of eight control serum samples had P4 levels exceeding the detection limit of 40 ng/ml.

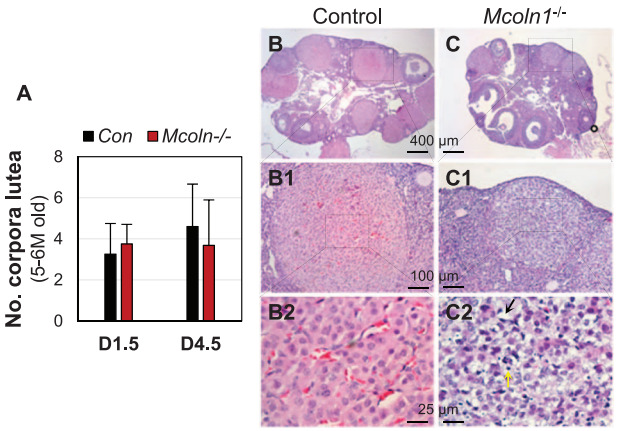

Figure 3. Numbers and histology of CLs at 5–6 months old. (A) Numbers of CLs in control (Con) and *Mcoln1*$^{-/-}$ ovaries on D1.5 and D4.5. N = 4 (D1.5) and 10–20 (D4.5); error bar, standard deviation. (B, B1, B2) Control. (C, C1, C2) *Mcoln1*$^{-/-}$. (B1 and C1) Corpus luteum enlarged from (B) and (C), respectively; (B2 and C2) Luteal cells enlarged from (B1) and (C1), respectively; scale bar: 400 μm (B–C), 100 μm (B1–C1), or 25 μm (B2–C2); yellow arrow in (C2): cell debris; black arrow in (C2): vacuolated cell. H & E staining.

Comparable numbers of CLs in *Mcoln1*$^{-/-}$ and control mice

Since P4 is mainly synthesized in the corpus luteum (CL, plural corpora lutea), which develops in the ovulated follicles during early pregnancy, P4 deficiency in the *Mcoln1*$^{-/-}$ females is an indication of defective CL. We examined the presence of CLs in the *Mcoln1*$^{-/-}$ ovaries at 5–6 months old. The numbers of CLs were comparable between control and *Mcoln1*$^{-/-}$ groups on both D1.5 and D4.5 (Figure 3A). Together with the comparable mating activities between control and *Mcoln1*$^{-/-}$ females (Figure 1A and B), these data indicate no obvious defects in ovulation and subsequent formation of CLs in the *Mcoln1*$^{-/-}$ females, and their P4 deficiency on D4.5 (Figure 2) was most likely a local defect in the CL.

Expression of TRPML1 in ovary

Immunohistochemistry indicated no specific staining in the D3.5 wild type mouse ovary of negative control (Figure 4A). There was differential expression of TRPML1 in the D3.5 wild type

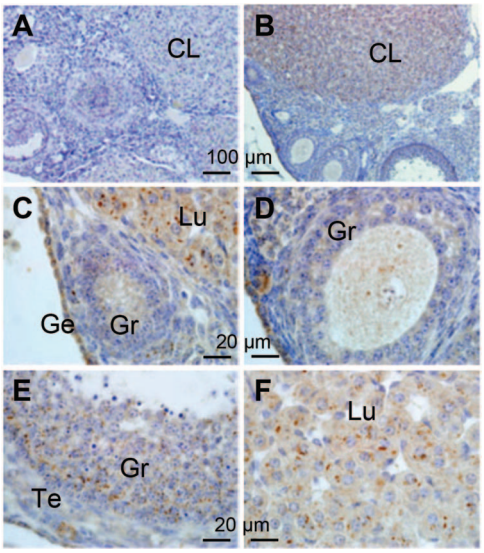

Figure 4. Detection of TRPML1 in D3.5 wild type mouse ovary using immunohistochemistry. (A) Negative control without primary antibody. (B–F) Transient receptor potential cation channel, mucolipin subfamily, member 1 expression in the ovary, with enlarged view of a primary follicle (C), a pre-antral follicle (D), an antral follicle (E), and a corpus luteum (F). CL: corpus luteum; Lu: luteal cells; Gr: granulosa cells; Te: theca cells; Ge: germinal epithelium; scale bar: 100 μm (A and B) or 20 μm (C and F); TRPML1 signal: brown staining; hematoxylin counterstaining: blue.

mouse ovary, which contained follicles at different stages and CLs (Figure 4B). TTRPML1 had a basal level of expression in the primary (Figure 4C) and pre-antral follicles, as well as in the oocyte (Figure 4D). TRPML1 was detected as granules in the granulosa cells but not theca cells of the antral follicle (Figure 4E). It had the highest expression level in the luteal cells as brown dots (Figure 4C and F), often larger than the granules detected in the granulosa cells of the antral follicle (Figure 4E). It appeared that TRMPL1 had basal levels of expression in the endothelial cells in the CL (Figure 4F). TRPML1 was also detectable in the germinal epithelium of the ovary (Figure 4C and D). This expression pattern of TRPML1 was consistent with a local function of TRPML1 in the CL, suggested by the normal mating activity (Figure 1A and B) and comparable numbers of CLs (Figure 3A) but P4 deficiency (Figure 2) in the *Mcoln1*$^{-/-}$ females.

Disrupted morphology in *Mcoln1*$^{-/-}$ corpus luteum

Histology of the D4.5 ovaries from the 5 months old mice in Figure 1 showed the presence of follicles at different stages and CLs in both WT and *Mcoln1*$^{-/-}$ ovaries (Figure 3B and C). The *Mcoln1*$^{-/-}$ CL had less defined corpus luteal cord formation and vasculature compared to the control CL (Figure 3B1–C2), which could also be indicated by the expression pattern of collagen IV (Col IV) (Figure 5). Collagen IV is a marker of the basal lamina of endothelial cells and it is highly expressed in the CL but absent in the follicles (Figure 5A and B) [28]. Immunofluorescence of Col IV revealed higher expression level of Col IV in the CLs than in the interstitial compartment of 5–6 months old D3.5 control ovaries (Figure 5A and data not shown), but such differential expression pattern was not observed in age-matched D3.5 *Mcoln1*$^{-/-}$ ovaries, which had comparable overall expression levels between the CLs and the interstitial compartment (Figure 5B and data not shown). The relative intensity of Col IV staining in the CLs normalized by that in the interstitial compartment of the same section was shown in Figure 5C. In addition to the overall reduced expression level of Col IV in the *Mcoln1*$^{-/-}$ CL (Figure 5C), the Col IV expression pattern was also disorganized in the *Mcoln1*$^{-/-}$ CL (Figure 5B1) compared to the control, which showed more organized and continuous staining (Figure 5A1). Besides the disrupted overall CL structure in the histology (Figure 3C1), there were additional abnormalities in the *Mcoln1*$^{-/-}$ CL, such as cellular vacuolization and presence of cell debris, indicative of cell degeneration (Figure 3C2).

Lipid accumulation in *Mcoln1*$^{-/-}$ corpus luteum

Mutations in *MCOLN1* cause lysosomal storage disorder MLIV, which is associated with lipid accumulation [33, 34]. We used Nile Red staining to detect lipid droplets in the CL [28]. Nile Red staining of D3.5 ovaries showed bright dots, which represented lipid droplets that contain cholesterol, the precursor for P4 synthesis [21], in the ovaries from 5 to 6 months old control and *Mcoln1*$^{-/-}$ mice (Figure 6). In a low magnification, the staining in the control CLs was relatively lighter than that in the surrounding interstitial compartment (Figure 6A); and the staining in the *Mcoln1*$^{-/-}$ CLs could be lighter than (Figure 6B, similar as in the control CLs (Figure 6A)) or comparable to (Figure 6C) that in the surrounding interstitial compartment. In a high magnification, the sizes of the lipid droplets were relatively similar in the control CLs and the lipid droplets with larger sizes appeared to be on the periphery of the cells (Figure 6A1); while the lipid droplets in the *Mcoln1*$^{-/-}$ CLs were often larger, in a range shown in Figure 6B1 and C1. Quantification data revealed comparable numbers of lipid droplets per area between control and *Mcoln1*$^{-/-}$ CLs (Figure 6D) and increased average size of lipid droplets in the *Mcoln1*$^{-/-}$ CLs compared with the control CLs (Figure 6E). These data demonstrate that there was lipid accumulation in the *Mcoln1*$^{-/-}$ CLs.

Reduction of mitochondrial density and StAR expression in *Mcoln1*$^{-/-}$ corpus luteum

The rate-limiting step of P4 synthesis takes place in the mitochondria and is the transport of cholesterol from outer to inner mitochondrial membrane by StAR (steroidogenic acute regulatory protein) [21, 35]. We used a mitochondrial marker heat shock protein 60 (HSP60) to label mitochondria in the CL using immunofluorescence (Figure 7). In the D4.5 control ovaries, the strongest labeling of HSP60 was detected in the CLs and the interstitial compartment, and the HSP60 labeling was much weaker in the follicles at 2 months and 6 months old (Figure 7A and A1). In the 2 months old D4.5 *Mcoln1*$^{-/-}$ ovaries, the strongest HSP60 labeling was detected in the CLs and/or the interstitial compartment (data not shown); while in the 6 months old D4.5 *Mcoln1*$^{-/-}$ ovaries, the HSP60 labeling was consistently lower in the CLs than that in the interstitial compartment (Figure 7B and B1). Compared with the age-matched control, the relative HSP60 staining in the CLs normalized by that in the interstitial compartment was significantly reduced in the D4.5 *Mcoln1*$^{-/-}$ ovaries at both 2 months and 6 months old. These results demonstrate reduced mitochondrial density in the *Mcoln1*$^{-/-}$ CL.

Figure 8 showed *in situ* hybridization of StAR in the D4.5 ovaries. There was strong staining in a CL of a pseudo-pregnant control ovary (Figure 8A and A1), strong staining in the CLs of a

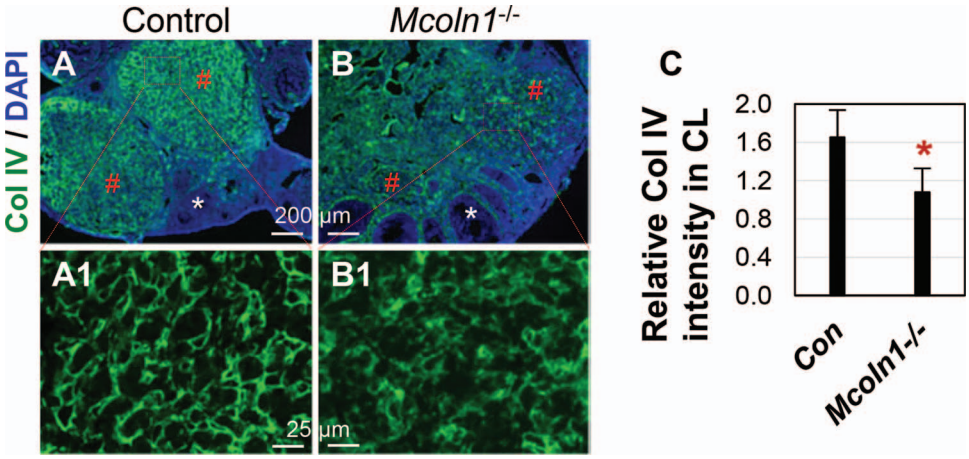

Figure 5. Immunofluorescence detection of collagen IV (Col IV) in corpra lutea of D3.5 control and *Mcoln1*$^{-/-}$ mice. (A) Control ovary. (B) *Mcoln1*$^{-/-}$ ovary. (A1 and B1) representative images of a corpus luteum enlarged from A and B, respectively; green: Col IV staining; blue: DAPI staining of nuclei; red #: corpus luteum; white *: follicle; scale bar: 200 μm (A–B) or 50 μm (A1–B1). (C) Relative intensity of Col IV staining in the CL/interstitial tissue in the ovary. N = 3–5; * $P < 0.05$; error bar, standard deviation.

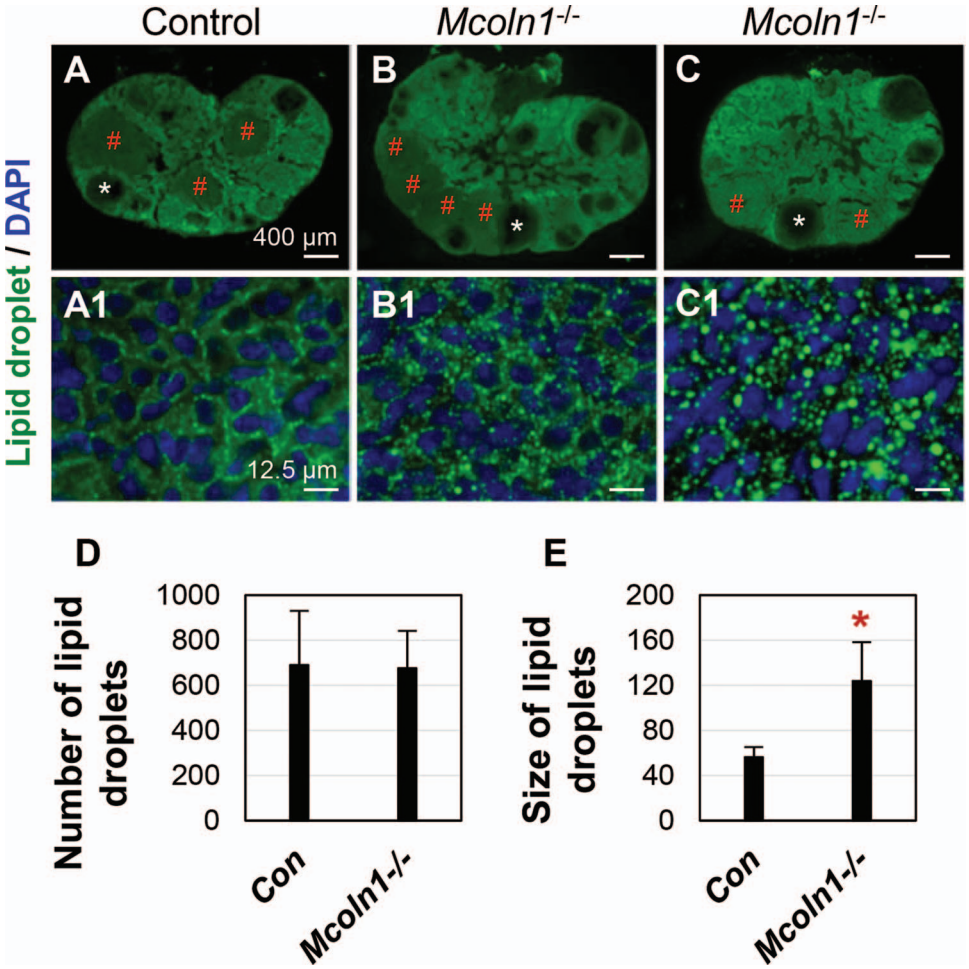

Figure 6. Nile red staining of lipid droplets in D3.5 control and *Mcoln1*$^{-/-}$ ovaries. (A) Control ovary. (B) A *Mcoln1*$^{-/-}$ ovary with mild lipid accumulation. (C) A *Mcoln1*$^{-/-}$ ovary with severe lipid accumulation. (A1–C1) Representative images of luteal cells enlarged from (A) to (C), respectively; green: Nile red staining of lipid droplets; blue, DAPI staining of nuclei; red #: corpus luteum; white *: follicle; scale bar: 400 μm (A–C) or 12.5 μm (A1–C1). (D) Number of lipid droplets in a standard reference frame (1041×780 pixel image). (E) Size of lipid droplets (square pixels). (D and E) N = 5; * $P < 0.05$; error bar, standard deviation.

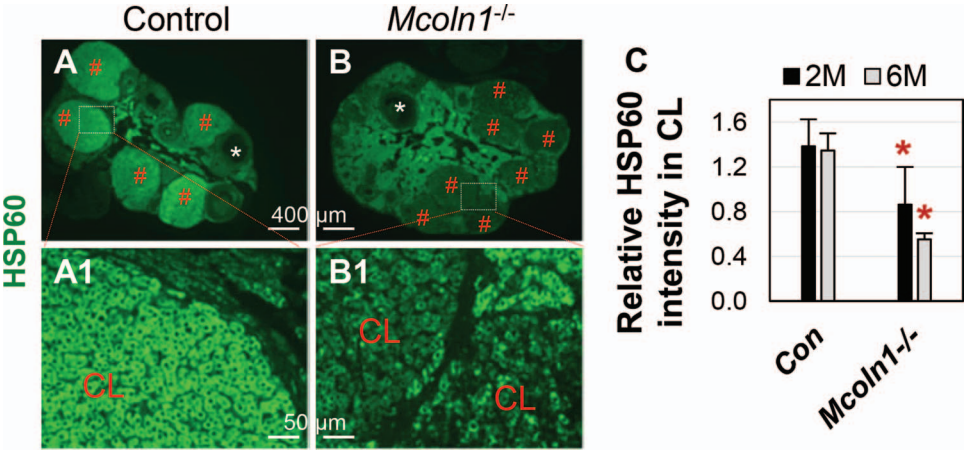

Figure 7. Immunofluorescence detection of a mitochondrial marker heat shock protein 60 (HSP60) in D4.5 control and *Mcoln1*$^{-/-}$ ovaries. A. Control ovary. B. *Mcoln1*$^{-/-}$ ovary. A1 and B1: representative images of CLs enlarged from A and B, respectively; green: HSP60 staining; red #: corpus luteum; white *: follicle; scale bar: 400 μm (A–B) or 50 μm (A1–B1). C. Relative intensity of HSP60 staining in the CL/interstitial compartment in the ovary. N=3–4; * $P < 0.05$, *compared to age-matched control; error bar, standard deviation.*

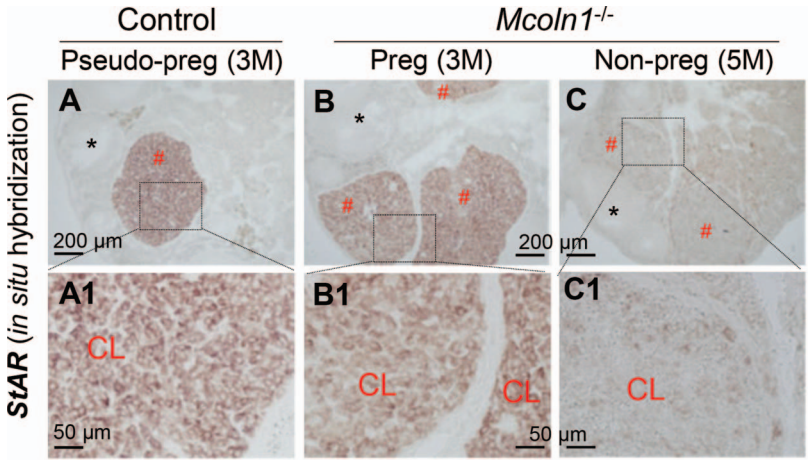

Figure 8. Detection of StAR mRNA expression in D4.5 ovaries by *in situ* hybridization using a StAR antisense probe. A. StAR expression in an ovary of a 3 months old pseudo-pregnant control mouse. B. StAR expression in an ovary of a 3 months old pregnant *Mcoln1*$^{-/-}$ mouse. C. StAR expression in an ovary of a 5 months old non-pregnant *Mcoln1*$^{-/-}$ mouse. A1-C1: Enlarged from the boxed area in A–C, respectively; red #: corpus luteum; black *: follicle; scale bar: 200 μm (A–C) or 50 μm (A1–C1); no specific staining in a control section using a StAR sense probe (data not shown).

fertile 3 months old *Mcoln1*$^{-/-}$ mouse (Figure 8B and B1), but weak staining in the CLs of an infertile 5 months old *Mcoln1*$^{-/-}$ mouse with P4 deficiency (Figure 8C and C1), in which only a few luteal cells had detectable level of StAR expression (Figure 8C1). Reduced StAR expression supports impaired steroidogenesis in the infertile *Mcoln1*$^{-/-}$ mice with P4 deficiency.

Discussion

Mutations in *MCOLN1*, which encodes a lysosomal counter ion channel TRPML1, cause a lysosomal storage disorder MLIV with a slow onset. Mucolipidosis type IV is progressive in humans and mice [1, 6–9]. In the *Mcoln1*$^{-/-}$ MLIV mouse model, the progressiveness is manifested in neurologic, gastric, and ophthalmologic aspects [9]. For example, *Mcoln1*$^{-/-}$ mice do not show obvious differences in growth, appearance, or behavior at 3 months old; however, they begin to show lethargy at 6 months old, and many of them quickly progress to total hind-limb paralysis and death within a couple of months [9]. The fertility of *Mcoln1*$^{-/-}$ female mice also shows such kind of progressiveness, with loss of fertility within 6 months old, before the manifestation of paralysis. The loss of female fertility accompanies with P4 deficiency. P4 is mainly produced in the CL during early pregnancy. Corpus luteum is a temporary endocrine structure normally developed at the site of ovulated follicle. It is puzzling why such a temporary structure also follows the overall progressive deterioration in *Mcoln1*$^{-/-}$ female mice.

TRPML1 is mainly detected in the granulosa cells of the antral follicle and luteal cells of the CL but its expression level in the earlier stage follicles is relatively low in the wild type ovary. This expression pattern supports the phenotype in the *Mcoln1*$^{-/-}$ ovary that there is no obvious defect in follicle development and the defects in the ovary are mainly seen in the CL. The comparable mating activities and numbers of CLs between age-matched control and *Mcoln1*$^{-/-}$ female mice, the expression pattern of TRPML1 in the wild type ovary, and the defects in the *Mcoln1*$^{-/-}$ CL support a local function of TRPML1

in the CL instead of neuroendocrine defect for P4 deficiency in the *Mcoln1*$^{-/-}$ females. It has been shown that follicle development is associated with decreased activities of lysosomal enzymes in the follicles of goat ovary [36]. This observation [36] together with low level expression of TRPML1 in the early stage of follicles and normal follicle development in the *Mcoln1*$^{-/-}$ ovary in our study suggest that lysosomes may not be essential for follicle development. Although TRPML1 has a relative high level of expression in the granulosa cells of the antral follicle, which will undergo rupture to release the oocyte during ovulation, and ovulation is associated with increased concentration of lysosomal enzymes in the ovarian bursa fluid [19], it would suggest that lysosomes, and potentially TRPML1 on lysosomal membrane, may play an important role in ovulation. However, *Mcoln1*$^{-/-}$ females at 5–6 months old had comparable numbers of CLs as the control, indicating that TRPML1 is not essential for ovulation and CL formation. Since vacuolization in the granulosa cells of the antral follicle (data not shown) is not common but vacuolization in the luteal cells is extensive in the *Mcoln1*$^{-/-}$ ovary at 5–6 months, it indicates that TRPML1 has a more profound role in the CL than in the antral follicle, which also expresses TRPML1.

In the CL, there are two dominant cell types, luteal cells and endothelial cells [37, 38]. Since TRPML1 is mainly detected in the wild type luteal cells but not endothelial cells, it is reasonable to conclude that the phenotypes observed in the *Mcoln1*$^{-/-}$ CL are mainly contributed by the function of TRPML1 in the luteal cells. The reduced level and disorganized expression of Col IV, a marker of the basal lamina of endothelial cells [28], indicate disorganized vasculature in the *Mcoln1*$^{-/-}$ CL, which is most likely a secondary effect from disorganized and degenerating luteal cells.

The luteal cells in the *Mcoln1*$^{-/-}$ CL are degenerating or have degenerated, indicated by the presence of cell debris. Defective lysosomes and defective mitochondria could both contribute to luteal cell degeneration. There is extensive luteal cell vacuolization in the *Mcoln1*$^{-/-}$ CL. Vacuolization is also detected in the gastric epithelial cells of the *Mcoln1*$^{-/-}$ mice and is formed by enlarged vesicles, most likely autophagic vacuoles, in the cytoplasm of gastric epithelial cells [9]. Although ultrastructural analysis of the luteal cells in the *Mcoln1*$^{-/-}$ CL has not been performed, some shared mechanisms are expected for the vacuolization in different cells of *Mcoln1*$^{-/-}$ mice and MLIV patients. Since TRPML1 is required for efficient fusion of autophagosomes with lysosomes, TRPML1 deficiency leads to impaired autophagosomal degradation and subsequent accumulation of autophagosomes in *Mcoln1*$^{-/-}$ mice and MLIV patients [9, 39]. Since TRPML1 deficiency also leads to the accumulation of larger lipid droplets that will be cleared during histological process of the ovarian sections, the accumulated lipid droplets, which may or may not be in the autophagosomes [40], most likely also contribute to the vacuoles seen in the histology of *Mcoln1*$^{-/-}$ CL. In addition to impaired autophagosomal degradation, which could lead to degenerative cell death, it has been reported that TRPML1 deficiency is also related to mitochondrial fragmentation, which will also contribute to progressive cell degeneration [41]. Indeed, there is a dramatic reduction of expression of a mitochondrial marker HSP60 in *Mcoln1*$^{-/-}$ CLs. Although the approach used in this study (immunofluorescence) is not suitable for determining mitochondrial integrity, such as mitochondrial fragmentation, the reduced expression of HSP60 would suggest mitochondrial dysfunction.

Since lipid droplets contain the precursor cholesterol for P4 synthesis [21], the accumulated lipid droplets in *Mcoln1*$^{-/-}$ CLs would imply that P4 deficiency is not due to insufficient precursor for P4 synthesis in *Mcoln1*$^{-/-}$ luteal cells. Since the rate-limiting step of P4 synthesis, which is the transport of cholesterol from outer to inner mitochondrial membrane by StAR [21], occurs in the mitochondria of luteal cells in the CL, the reduction of HSP60 in *Mcoln1*$^{-/-}$ CL would suggest impaired mitochondrial function for P4 synthesis, which is supported by the reduced expression of StAR in the CLs of *Mcoln1*$^{-/-}$ mice with P4 deficiency. Although the mechanisms of how TRPML1 deficiency leads to cell vacuolization, reduced StAR expression, and impaired mitochondrial function in the *Mcoln1*$^{-/-}$ luteal cells are unknown, luteal cell degeneration inevitably leads to P4 deficiency in *Mcoln1*$^{-/-}$ female mice.

There are two main findings in this study: (1) lysosomal counter ion channel TRPML1 plays an important role in the corpus luteum for progesterone synthesis and (2) lysosomes are also important for luteal cell survival in addition to their known function in luteal regression. Although the molecular mechanisms remain to be investigated, these findings provide novel insights into the regulation of luteal cells for progesterone synthesis, which is essential for pregnancy in mammals.

Acknowledgments

The authors thank the Office of the Vice President for Research, Interdisciplinary Toxicology Program, Department of Physiology and Pharmacology, and College of Veterinary Medicine at the University of Georgia, and the National Institutes of Health (NIH R01HD065939 (co-funded by ORWH and NICHD) and R03HD097384 to XY) for financial support. Serum P4 and E2 levels were determined at The University of Virginia Center for Research in Reproduction Ligand Assay and Analysis Core, which is supported by the Eunice Kennedy Shriver NICHD/NIH (NCTRI) Grant P50-HD28934.

Conflict of interest

The authors have declared that no conflict of interest exists.

References

1. Xu H, Ren D. Lysosomal physiology. *Annu Rev Physiol* 2015; **77**:57–80.
2. DiCiccio JE, Steinberg BE. Lysosomal pH and analysis of the counter ion pathways that support acidification. *J Gen Physiol* 2011; **137**:385–390.
3. Cao Q, Zhong XZ, Zou Y, Zhang Z, Toro L, Dong XP. BK channels alleviate lysosomal storage diseases by providing positive feedback regulation of lysosomal Ca(2+) release. *Dev Cell* 2015; **33**:427–441.
4. Li P, Gu M, Xu H. Lysosomal ion channels as decoders of cellular signals. *Trends Biochem Sci* 2018; **44**:110–124.
5. Di Paola S, Scotto-Rosato A, Medina DL. TRPML1: The Ca((2+))retaker of the lysosome. *Cell Calcium* 2018; **69**:112–121.
6. Venkatachalam K, Wong CO, Zhu MX. The role of TRPMLs in endolysosomal trafficking and function. *Cell Calcium* 2015; **58**:48–56.
7. Chandra M, Zhou H, Li Q, Muallem S, Hofmann SL, Soyombo AA. A role for the Ca2+ channel TRPML1 in gastric acid secretion, based on analysis of knockout mice. *Gastroenterology* 2011; **140**:857–867.
8. Wang W, Zhang X, Gao Q, Xu H. TRPML1: an ion channel in the lysosome. *Handb Exp Pharmacol* 2014; **222**:631–645.
9. Venugopal B, Browning MF, Curcio-Morelli C, Varro A, Michaud N, Nanthakumar N, Walkley SU, Pickel J, Slaugenhaupt SA. Neurologic, gastric, and opthalmologic pathologies in a murine model of mucolipidosis type IV. *Am J Hum Genet* 2007; **81**:1070-1083
10. Driancourt MA. Follicular Dynamics in Sheep and Cattle. *Theriogenology* 1991; **35**:55–79.
11. Banon P, Brandes D, Frost JK. Lysosomal enzymes in the rat ovary and endometrium during the estrous cycle. *Acta Cytol* 1964; **8**:416–425.

12. Dhanasekaran N, Sheela Rani CS, Moudgal NR. Studies on follicular atresia: lysosomal enzyme activity and gonadotropin receptors of granulosa cells following administration or withdrawal of gonadotropins in the rat. *Mol Cell Endocrinol* 1983; **33**:97–112.
13. Rosales-Torres AM, Avalos-Rodriguez A, Vergara-Onofre M, Hernandez-Perez O, Ballesteros LM, Garcia-Macedo R, Ortiz-Navarrete V, Rosado A. Multiparametric study of atresia in ewe antral follicles: histology, flow cytometry, internucleosomal DNA fragmentation, and lysosomal enzyme activities in granulosa cells and follicular fluid. *Mol Reprod Dev* 2000; **55**:270–281.
14. Alonso-Pozos I, Rosales-Torres AM, Avalos-Rodriguez A, Vergara-Onofre M, Rosado-Garcia A. Mechanism of granulosa cell death during follicular atresia depends on follicular size. *Theriogenology* 2003; **60**: 1071–1081.
15. Miyake Y, Matsumoto H et al. Expression and glycosylation with polylactosamine of CD44 antigen on macrophages during follicular atresia in pig ovaries. *Biology of reproduction* 2006; **74**:501–510.
16. Eykelbosh AJ, Van Der Kraak G. A role for the lysosomal protease cathepsin B in zebrafish follicular apoptosis. *Comp Biochem Physiol A Mol Integr Physiol* 2010; **156**:218–223.
17. Escobar ML, Echeverria OM, Ortiz R, Vazquez-Nin GH. Combined apoptosis and autophagy, the process that eliminates the oocytes of atretic follicles in immature rats. *Apoptosis* 2008; **13**:1253–1266.
18. Rodrigues P, Limback D, McGinnis LK, Plancha CE, Albertini DF. Multiple mechanisms of germ cell loss in the perinatal mouse ovary. *Reproduction* 2009; **137**:709–720.
19. Parr EL. Beta-galactosidase in rat ovarian bursa fluid at ovulation. *Biol Reprod* 1974; **11**:504–508.
20. Cajander S, Bjersing L. Further-Studies of Surface Epithelium Covering Preovulatory Rabbit Follicles with Special Reference to Lysosomal Alterations. *Cell and Tissue Research* 1976; **169**:129–141.
21. Christenson LK, Devoto L. Cholesterol transport and steroidogenesis by the corpus luteum. *Reprod Biol Endocrinol* 2003; **1**:90.
22. Savion N, Laherty R, Lui GM, Gospodarowicz D. Modulation of low density lipoprotein metabolism in bovine granulosa cells as a function of their steroidogenic activity. *J Biol Chem* 1981; **256**:12817–12822.
23. Zhang JY, Wu Y, Zhao S, Liu ZX, Zeng SM, Zhang GX. Lysosomes are involved in induction of steroidogenic acute regulatory protein (StAR) gene expression and progesterone synthesis through low-density lipoprotein in cultured bovine granulosa cells. *Theriogenology* 2015; **84**:811–817.
24. Gregoraszczuk EL, Sadowska J. Lysosomal acid phosphatase activity and progesterone secretion by porcine corpora lutea at various periods of the luteal phase. *Folia Histochem Cytobiol* 1997; **35**:35–39.
25. Aboelenain M, Kawahara M, Balboula AZ, Montasser Ael M, Zaabel SM, Okuda K, Takahashi M. Status of autophagy, lysosome activity and apoptosis during corpus luteum regression in cattle. *J Reprod Dev* 2015; **61**:229–236.
26. Xiao S, Diao H, Zhao F, Li R, He N, Ye X. Differential gene expression profiling of mouse uterine luminal epithelium during periimplantation. *Reprod Sci* 2014; **21**:351–362.
27. Xiao S, Li R, El Zowalaty AE, Diao H, Zhao F, Choi Y, Ye X. Acidification of uterine epithelium during embryo implantation in mice. *Biol Reprod* 2017; **96**:232–243.
28. El Zowalaty AE, Li R, Zheng Y, Lydon JP, DeMayo FJ, Ye X. Deletion of RhoA in progesterone receptor-expressing cells leads to luteal insufficiency and infertility in female mice. *Endocrinology* 2017; **158**: 2168–2178.
29. Ye X, Hama K, Contos JJ, Anliker B, Inoue A, Skinner MK, Suzuki H, Amano T, Kennedy G, Arai H, Aoki J, Chun J. LPA3-mediated lysophosphatidic acid signalling in embryo implantation and spacing. *Nature* 2005; **435**:104–108.
30. Diao H, Xiao S, Howerth EW, Zhao F, Li R, Ard MB, Ye X. Broad gap junction blocker carbenoxolone disrupts uterine preparation for embryo implantation in mice. *Biol Reprod* 2013; **89**:31.
31. Li R, Zhao F, Diao H, Xiao S, Ye X. Postweaning dietary genistein exposure advances puberty without significantly affecting early pregnancy in C57BL/6J female mice. *Reprod Toxicol* 2014; **44**:85–92.
32. Zhao F, Zhou J, El Zowalaty AE, Li R, Dudley EA, Ye X. Timing and recovery of postweaning exposure to diethylstilbestrol on early pregnancy in CD-1 mice. *Reprod Toxicol* 2014; **49C**:48–54.
33. Wakabayashi K, Gustafson AM, Sidransky E, Goldin E. Mucolipidosis type IV: an update. *Mol Genet Metab* 2011; **104**:206–213.
34. Soyombo AA, Tjon-Kon-Sang S, Rbaibi Y, Bashllari E, Bisceglia J, Muallem S, Kiselyov K. TRP-ML1 regulates lysosomal pH and acidic lysosomal lipid hydrolytic activity. *J Biol Chem* 2006; **281**: 7294–7301.
35. Manna PR, Dyson MT, Stocco DM. Regulation of the steroidogenic acute regulatory protein gene expression: present and future perspectives. *Mol Hum Reprod* 2009; **15**:321–333.
36. Ballesteros LM, Rosales AM et al. Activity, compartmentation and subcellular distribution of lysosomal enzymes during follicular maturation in the goat. *Animal Reproduction Science* 1992; **28**:129–139.
37. Davis JS, Rueda BR, Spanel-Borowski K. Microvascular endothelial cells of the corpus luteum. *Reprod Biol Endocrinol* 2003; **1**:89.
38. Miyamoto A, Shirasuna K, Shimizu T, Matsui M. Impact of angiogenic and innate immune systems on the corpus luteum function during its formation and maintenance in ruminants. *Reprod Biol* 2013; **13**:272–278.
39. Vergarajauregui S, Puertollano R. Mucolipidosis type IV: the importance of functional lysosomes for efficient autophagy. *Autophagy* 2008; **4**:832–834.
40. Deretic V.. Autophagosomes and lipid droplets: no longer just chewing the fat. *EMBO J* 2015; **34**:2111–2113.
41. Eichelsdoerfer JL, Evans JA, Slaugenhaupt SA, Cuajungco MP. Zinc dyshomeostasis is linked with the loss of mucolipidosis IV-associated TRPML1 ion channel. *J Biol Chem* 2010; **285**:34304–34308.